7th International Symp. on Ballistics 1983

PENETRATION OF COMPRESSIBLE MATERIALS BY SHAPED-CHARGE JETS

William J. Flis and Pei Chi Chou

Dyna East Corporation
3132 Market Street
Philadelphia, PA 19104-2855
U.S.A.

When a shaped-charge jet penetrates a highly compressible material, such as a plastic or liquid, the total penetration may be significantly less, by as much as 50%, than that predicted by the classical incompressible, hydrodynamic theory of jet penetration. In this paper, the compressible jet penetration model of Haugstad and Dullum [J. Appl. Phys., 52, 5066 (1981)] is generalized to include a complete equation of state of the Mie-Gruneisen or Tillotson type. The model is further extended to the more realistic case of a stretching jet. Calculated results indicate that compressibility effects can account for as much as 50% degradation in penetration compared to the classical theory.

I. INTRODUCTION

At the high impact velocities of shaped-charge jets, both the jet and target materials are subjected to extremely high pressures and are appreciably compressed. In the past, effects of compressibility in jet penetration have been discounted [1, 2] because they are not important for a copper jet impacting a steel target; the similarity in density and compressibility of the two materials leads to the result that the penetration velocity is about half the impact velocity, whether compressibility is considered or not. But in such highly compressible target materials of current interest as plastics and liquids, the penetration is significantly less, by up to 50% [3], than that calculated from the classical one-dimensional incompressible model of penetration [4, 5]. It is also important that, since the effect of compressibility on penetration increases with jet velocity, the most efficient jet penetrator may not have the highest velocity; this will effect modern trends in armor and warhead design.

This paper is an analytical study of compressibility effects in jet penetration. The one-dimensional, compressible, steady-flow model of Haugstad and Dullum [6] is modified to include a complete equation of state, and extended to the more practical case of a stretching jet. At sufficiently high impact velocities, shock waves may exist in the jet and/or target, and are included in the model. Transitions in the velocities and thermodynamic states of each material occur across the shock according to the Rankine-Hugoniot conditions, and from the shock to the stagnation point according to the compressible Bernoulli equation. From these equations, the penetration velocity and penetration per unit length of jet may be calculated for any jet velocity. The penetration of a stretching jet, of linear velocity distribution, is derived by integration over the length of the jet. The stretching jet is a close approximation of the short-standoff behavior of an actual shaped-charge jet, and its consideration is important for warhead and armor design.

In the next section, the basic theory for compressible penetration by a uniform-velocity jet is described. In Section III, the theory is extended to the case of a stretching jet. Then, in Section IV, some calculated results are presented and discussed. Finally, in Section V, a few conclusions are made.

II. BASIC THEORY

In this section, the basic theory of the compressible jet-penetration model is described. Figure 1 is an illustration of jet penetration. The jet, having a velocity V, propagates a crater into the target at a velocity U, called the penetration velocity, as shown in Figure 1(a). At sufficiently high jet velocities, shock waves are created in the target and the jet. In Figure 1(b), this process is viewed in moving coordinates fixed to the bottom of the crater, which now appears as a stagnation point in the flow. Jet material approaches this point at velocity (V - U) and target material at velocity U. We define, along the central streamline, station 0_t in the undisturbed target material ahead of the standing shock wave, station 1_t behind the shock, and station 2_t in the target material at the stagnation point; corresponding stations 0_j, 1_j, and 2_j are defined in the jet.

Changes in the velocity and thermodynamic state of each material across the shock are governed by the Rankine-Hugoniot conditions. Along the central streamline, the flow is normal to each shock, with properties as shown in Figure 2. Across each shock, the governing equations are conservations of mass,

$$\rho_0 U_s = \rho_1 (U_s - U_p) \tag{1}$$

conservation of momentum,

$$p_0 + \rho_0 U_s^2 = p_1 + \rho_1 (U_s - U_p)^2 \tag{2}$$

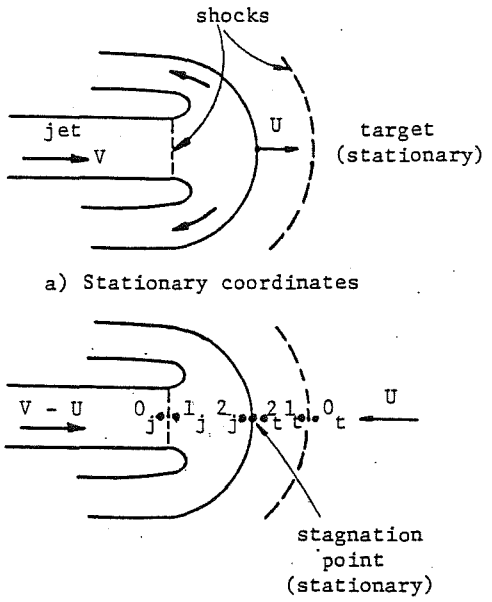

a) Stationary coordinates

b) Moving coordinates

Figure 1. Compressible jet penetration.

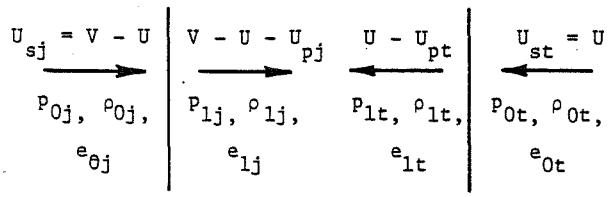

a) shock in jet b) shock in target

Figure 2. Properties across standing shock waves.

and conservation of energy,

$$e_0 + \frac{p_0}{\rho_0} + \frac{1}{2} U_s^2 = e_1 + \frac{p_1}{\rho_1} + \frac{1}{2} (U_s - U_p)^2 \qquad (3)$$

where ρ is density, p is pressure, U_s is the shock velocity relative to the undisturbed material ahead of it, U_p is the particle velocity imparted by the shock, and e is specific internal energy. U_s and U_p are defined for each material in Figure 2.

Completion of the description of the material behavior at the shock requires the equation of state, $p = p(\rho, e)$. For simplicity, we may substitute here the linear shock-velocity-particle-velocity Hugoniot,

$$U_s = C_0 + bU_p \qquad (4)$$

where C_0 is the bulk sound speed, and b is an empirical constant. This equation has been found satisfactory for many solid materials.

Changes in properties between stations 1 and 2 in each material may be determined by assuming that the flow is steady and that the material is continuously decelerated and adiabatically compressed. Since the axis of the flow is a streamline, the motion is described by the compressible form of Bernoulli's equation,

$$\frac{1}{2} \mathcal{V}^2 + \frac{p}{\rho} - \int p\,dv = \text{constant} \qquad (5)$$

where $\mathcal{V}$ is the local particle velocity and $v = 1/\rho$ is the specific volume. In the moving coordinates of Figure 1(b), the particle velocity is $U_s - U_p$ behind the shock (station 1) and zero at the stagnation point (station 2). Therefore,

$$\frac{1}{2} (U_s - U_p)^2 + \frac{p_1}{\rho_1} = \frac{p_2}{\rho_2} - \int_1^2 p\,dv \qquad (6)$$

If, for each material, it is assumed that the pressure is a function of specific volume only (barotropic), the last term is integrable. But for a general equation of state, of functional form

$$p = p(\rho, e) \qquad (7)$$

an additional condition is required. For an adiabatic (i.e., isentropic) process, conservation of energy requires that

$$de = - p\,dv \qquad (8)$$

along the path from station 1 to station 2.

The final equation is the requirement of equilibrium of pressure across the material interface at the stagnation point,

$$p_{2j} = p_{2t} \qquad (9)$$

The above development is similar to that presented in [6] with two exceptions. First, it is implied in [6] that the compressible Bernoulli's equation (5) can be derived from considerations of conservation of energy, and stated that it is therefore applicable to non-isentropic flow, such as through a shock. However, Bernoulli's equation is properly derived by integration along a streamline of Euler's equation for continuous steady flow; therefore, it is not applicable to a discontinuous phenomenon, such as a shock. Furthermore, since Bernoulli's equation is not a statement of conservation of energy but actually an integrated momentum equation, the type of thermodynamic process involved (isentropic or otherwise) is immaterial.

In [6], Bernoulli's equation was incorrectly applied across the shock in place of the Hugoniot energy equation (3). These equations are not identical because, in general,

$de = Tds - pdv$, and thus, the unlike terms in these equations are not equal,

$$e_1 - e_0 \neq -\int_0^1 pdv$$

since entropy is not constant across the shock.

The second difference is that, in [6], the constitutive equation of Murnaghan [7]

$$1 + \beta(4b - 1)(p - p_1) = (v_1/v)^{4b-1}$$

where β is the adiabatic compressibility and b is defined in equation (4), is used between stations 1 and 2. This equation involves only two thermodynamic state variables, pressure and specific volume, whereas three variables are related in a full equation of state. Therefore, some thermodynamic process is implied in Murnaghan's equation. In Murnaghan's original paper [7], the equation was proposed as a fit to data from Bridgman's well-known experiments [8], which were quasi-static and therefore followed an isothermal process. In [6], Murnaghan's equation was used to describe the isentrope. However, values chosen for the empirical constants in the equation are shock properties, fitting the equation to the Hugoniot, which is neither isothermal nor isentropic. Consequently, there is some doubt as to the applicability of Murnaghan's equation in this instance.

In the present study, this difficulty is alleviated by using a full equation of state in combination with the energy equation and the adiabatic condition. In particular, for solids, we have chosen the widely accepted equations of state of Mie-Gruneisen [9]

$$p = (C\mu + D\mu^2 + S\mu^3)\left(1 - \frac{\Gamma\mu}{2}\right) + \Gamma\rho e$$

where

$$\mu \equiv \frac{\rho}{\rho_0} - 1$$

and of Tillotson [10],

$$p = A\mu + B\mu^2 + e\rho\left[a + \frac{b}{e/(e_0\eta^2) + 1}\right]$$

where

$$\eta \equiv \rho/\rho_0$$

In addition, a high-pressure equation of state for water [11] has been incorporated.

The system of equations (1) - (4) and (6) - (9) is solved by the method of successive substitution. For a given jet velocity V, a value of penetration velocity U is guessed from, say, the incompressible Bernoulli's equation. Properties behind the shocks (at stations 1t and 1j) are determined from equations (1) - (4). Then, properties at the stagnation point are computed from equations (6) - (8); with a general equation of state, the integral in equation (6) must be evaluated numerically while satisfying the adiabatic condition, equation (8). Now, as shown in [6], combining equations (2), (6) and (9) yields

$$\left(\frac{V-\mathcal{V}}{U}\right)^2 = \frac{\rho_{ot}}{\rho_{oj}}\left\{\gamma + \frac{(\gamma - 1)p_o}{\frac{1}{2}\rho_{ot}U^2} + \frac{\rho_{oj}(e_{2j} - e_{oj}) - \gamma\rho_{ot}(e_{2t} - e_{ot})}{\frac{1}{2}\rho_{ot}U^2}\right\} \quad (10)$$

$$\equiv \frac{\rho_{ot}}{\rho_{oj}}\psi^{-1}$$

where

$$\gamma \equiv \frac{\rho_{2t}}{\rho_{2j}}\frac{\rho_{oj}}{\rho_{ot}}$$

If compressibility effects are neglected, this equation reduces to the classical theory of [4] for which $\psi = 1$. Results calculated using the assumed value of U are substituted into the right-hand side of the above equation, and a new value of U is determined. The process is repeated until successive values of U are the same.

The penetration per unit length of jet is

$$\frac{P}{L} = \frac{U}{V - U}$$

The ratio, then, of penetration predicted by the compressible model to that by the classical theory is

$$\frac{P_{compressible}}{P_{incompressible}} = \sqrt{\psi}$$

The deviation of this quantity from unity represents the magnitude of the compressibility effect on the penetration of a uniform-velocity jet.

III. STRETCHING JET

In this section, the compressible penetration model is extended to the case of a stretching jet. It is assumed that the jet is continuous (unbroken) and that the steady-flow model presented above is valid at each instant of this unsteady case. If it is further assumed that the velocity distribution of the jet is linear with position, then the virtual-origin approach of [1] may be used. While the model is also applicable to jets of arbitrary velocity distribution, the linear restriction allows the presentation here of some useful results in terms of just a few parameters.

Figure 3 is a space-time diagram of penetration by a stretching jet. If, at some early time t_e, the jet has a linear velocity distribution with respect to distance x, then the jet appears to emanate from a single point, called the virtual origin.

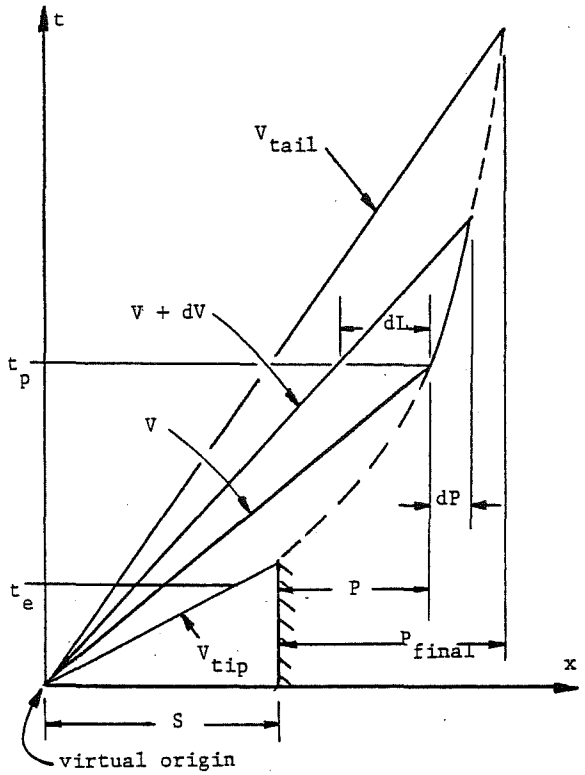

Figure 3. Penetration by a stretching jet.

Now, let dL represent an incremental length of jet at the time of penetration. Then, as shown in Figure 3, the increment of penetration due to this length of jet is, by kinematics,

$$dP = \frac{U}{V - U} dL \tag{11}$$

If dV is the change in jet velocity across dL, then

$$dL = -t_p dV \tag{12}$$

where t_p, the time of penetration by dL, is

$$t_p = \frac{P + S}{V} \tag{13}$$

where S is the distance from the virtual origin to the face of the target.

Combination of equations (11) - (13) and integration over the entire penetration process yields

$$\int_0^{P_{final}} \frac{dP}{P+S} = -\int_{V_{tip}}^{V_{tail}} \frac{U}{V - U} \frac{dV}{V} \tag{14}$$

From the compressible penetration model, we have, by equation (10),

$$\frac{U}{V - U} = k\sqrt{\psi}$$

where $k \equiv \sqrt{\rho_j/\rho_t}$ and $\psi = \psi(V)$ accounts for compressibility effects. Substitution into equation (14) and integration yields

$$P_{compressible} = S[(\exp\Phi)^k - 1] \tag{15}$$

where

$$\Phi \equiv \int_{V_{tail}}^{V_{tip}} \frac{\sqrt{\psi}}{V} dV \tag{16}$$

This result may be compared with the penetration predicted by the incompressible model. If compressibility effects are neglected, $\psi = 1$, so that equation (15) reduces to

$$P_{incompressible} = S\left[\left(\frac{V_{tip}}{V_{tail}}\right)^k - 1\right] \tag{17}$$

Taking the ratio of equations (15) and (17) yields

$$\frac{P_{compressible}}{P_{incompressible}} = \frac{(\exp\Phi)^k - 1}{(V_{tip}/V_{tail})^k - 1} \tag{18}$$

The deviation of this ratio from unity represents the degree of effect of compressibility on the penetration of a stretching jet.

IV. CALCULATED RESULTS

In this section, a few calculated results are presented and discussed. First, a comparison is made using Murnaghan's equation with results presented in [6], in which a computational error has apparently been made. Second, results predicted by the model using the other equations of state are presented; a few cases are discussed in detail. Finally, calculations of the penetration by a stretching jet are presented.

Comparison with Haugstad and Dullum

The above theoretical development was written into a computer program. As a check, calculations were performed using Murnaghan's equation to compare with results presented in [6]. In Figure 4, these results are compared in terms of the ratio of penetration calculated from the compressible model to that predicted by the classical imcompressible theory. It may be seen, first, that both sets of calculations show little effect of compressibility for the case of a copper jet against a steel target and a significant effect for a Plexiglas target.

Second, while the results of the present calculation and those of [6] are identical when

the shocks are neglected, there is a significant difference when the shocks are included. Specifically, the present calculations attribute much less effect to the presence of the shocks. Similar results were obtained for targets of lead, platinum and aluminum. We believe that this difference arises from an error in the computations of [6], which we may explain as follows. Using Murnaghan's equation, the change in internal energy along the isentrope may be integrated exactly.

$$e_2 - e_1 = -\int_1^2 p\,dv = -\frac{v_1}{\beta q}\left\{p_1\beta q(X-1) + \frac{X^{1-q}}{1-q} - X - \frac{q}{1-q}\right\}$$

where

$$X \equiv v_2/v_1, \qquad q \equiv 4b - 1$$

When this result was first presented by Haugstad (equation (9) of [12]), the first term in the brackets was omitted. Now, when shocks are not present or not considered, this omission is of no consequence because $p_1 = p_o$, which is taken as zero. However, when shocks are present, this term is not negligible; the effect of its omission is to calculate too large an increase in internal energy along the isentrope, and thus to overestimate the effect of compressibility.

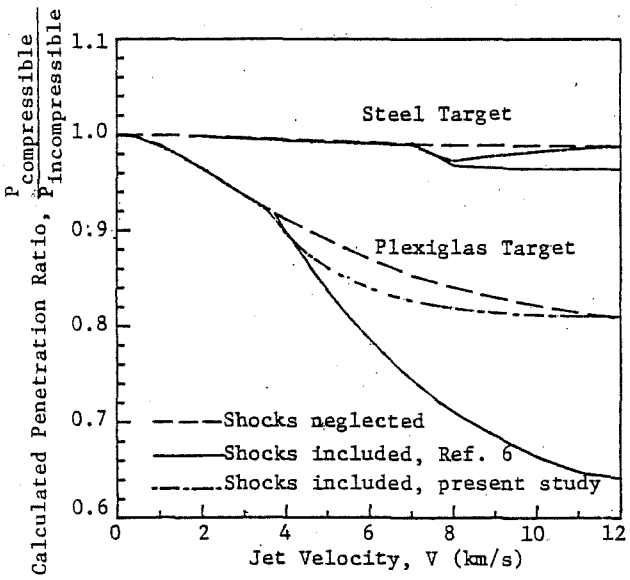

Figure 4. Effect of compressibility on penetration by a uniform-velocity copper jet using Murnaghan's equation, comparing calculations of Haugstad [6] with the present study.

Other Equations of State

Calculations using the compressible penetration model have been performed for several jet/target combinations using different equations of state. Material properties are listed in Table 1. The results of calculations for a uniform-velocity copper jet into steel and polyethylene targets, using the Murnaghan, Mie-Gruneisen and Tillotson equations of state, are shown in Figure 5, in which the ratio of compressible to incompressible penetration is plotted against jet velocity. For a steel target, the results are essentially the same for all three constitutive relations, and indicate that compressibility effects are negligible in this case. For a polyethylene target, there is some disparity among results calculated using the three equations, attributable to the wide variability in the mechanical properties of polyethylene. Furthermore, the polyethylene target shows a significant effect of compressibility, with as much as a 19% reduction in penetration compared to the classical theory.

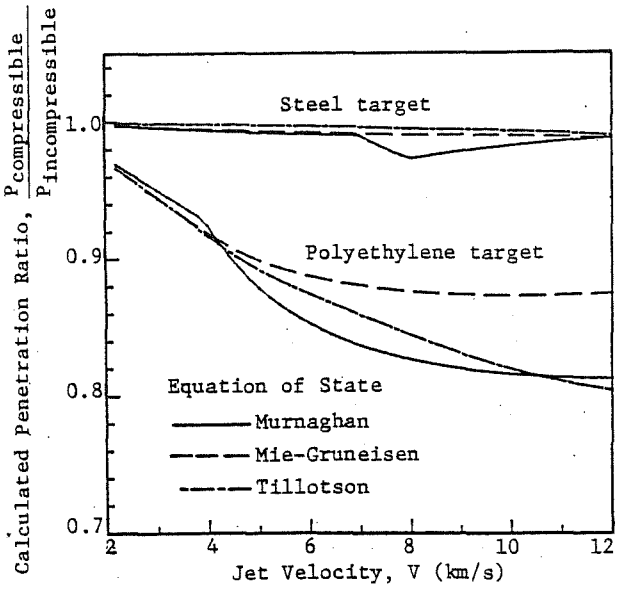

Figure 5. Effect of compressibility on penetration of a uniform-velocity copper jet into steel and polyethylene targets as predicted using different equations of state.

Figure 6 presents results of calculations using the Mie-Gruneisen equation of state for a uniform-velocity copper jet into several target materials. Note that for a platinum target, the compressible theory predicts more penetration per unit length of jet than the incompressible theory; this result may be attributed to the lower compressibility of platinum compared to copper. For targets of successively increasing compressibilities (steel, then aluminum, lead, Plexiglas and polyethylene), the compressible theory predicts successively greater reductions in penetration compared to the incompressible theory.

Table 1

Properties of Jet and Target Materials

Material	Copper	Steel	Lead	Aluminum	Platinum	Plexiglas	Polyethylene
Density, ρ_o (Mg/m^3)	8.93	7.84	11.36	2.70	21.37	1.186	0.92
Bulk sound speed, C_o(km/s)	3.920	3.596	2.100	5.440	3.636	2.745	2.931
Murnaghan Constants:							
$\beta(10^{-12}Pa^{-1})$	7.29	9.86	19.97	12.52	3.54	111.9	126.5
b	1.488	1.686	1.450	1.327	1.539	1.451	1.472
Mie-Gruneisen Constants:							
$C(10^{11}$ Pa)	1.372	1.014	0.501	0.799	2.825	0.0894	0.0790
$D(10^{11}$ Pa)	1.752	-0.2475	0.499	1.139	5.297	0.0457	0.0230
$S(10^{11}$ Pa)	5.64	10.74	2.019	1.398	9.26	0.436	0.434
Γ	1.96	1.69	2.20	2.09	2.62	0.80	0.86
Tillotson Constants:							
$a(10^{11}$ Pa)	1.39	1.17	0.466	0.750	-	-	0.075
$b(10^{11}$ Pa)	1.10	0.550	0.150	0.650	-	-	0.020
A	0.5	0.55	0.4	0.5	-	-	0.6
B	1.5	0.62	2.4	1.63	-	-	2.0
$e_o(10^{12}$J/kg)	0.325	0.175	0.020	0.050	-	-	0.07

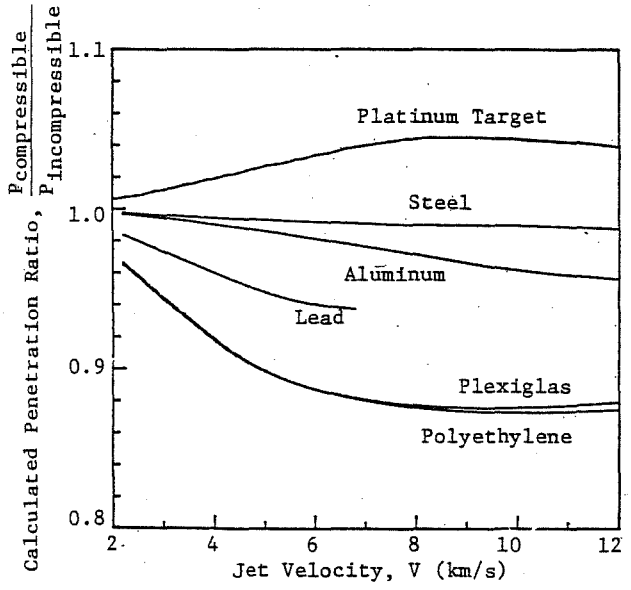

Figure 6. Effect of compressibility on penetration of a uniform-velocity copper jet into several materials as predicted using the Mie-Gruneisen equation of state.

Discussion of Results

The above results may be better understood by considering the changes in material states during the penetration process. Figure 7 is a plot of pressure and velocity states for a copper jet impacting a steel target at 7 km/s. This type of plot, commonly used to graphically describe one-dimensional transient impact (e.g., plate slap), can also illustrate steady-state penetration. Points 0_j at a velocity of 7 km/s and 0_t at zero velocity represent the undisturbed states of the jet and target, respectively. Conditions immediately after a transient one-dimensional impact are given by the intersection of the steel pressure-velocity Hugoniot drawn through point 0_t with the copper Hugoniot drawn backward through point 0_j.

For steady-state jet penetration, note first that, since the jet and target flow velocities relative to the stagnation point are both subsonic (i.e., $V - U < C_{oj}$ and $U < C_{ot}$), no standing shocks are set up, so there is no distinction between stations 0_j and 1_j or between 0_t and 1_t. Now, the incompressible theory predicts that, as the jet and target materials flow toward the stagnation point, the pressure p and flow velocity v change continuously according to the incompressible Bernoulli's equation $p + \rho v^2/2 = \text{constant}$.

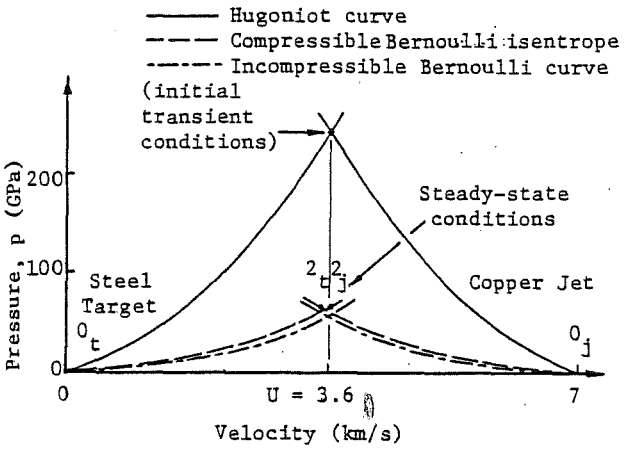

Figure 7. Pressure-velocity diagram for penetration of a copper jet into a steel target at 7 km/s.

At station 2_j and 2_t, the pressures and velocities must match, so that the conditions at the stagnation point are given by the intersection of the two Bernoulli's-equation curves. The velocity at this point is the penetration velocity $U_{incompressible}$ = 3.6 km/s.

If compressibility is taken into account, then the proper conditions along a streamline are the compressible Bernoulli's equation, $pv + \gamma^2/2 - \int pdv$ = constant, together with the equation of state (Mie-Gruneisen in this example) and the condition of constant entropy. This set of conditions, which defines the compressible isentrope, yields a slightly greater pressure increase between stations 0 and 2 than the incompressible theory, as shown in the figure. However, since copper and steel are nearly equally compressible (with bulk moduli 1.37 x 10^{11} Pa for copper and 1.04 x 10^{11} for steel), the net effect is that the compressible isentropes are each about an equal distance above the incompressible curves; thus, while the compressible curves intersect at a slightly higher pressure, the penetration velocity U is practically identical to the incompressible case (less than 1% difference). Since the penetration depth per unit length of jet is directly related to the penetration velocity (by equation (11)), it follows that the penetration calculated from the compressible theory is almost the same as from the incompressible theory.

Consider now a copper jet impacting a steel target at 9 km/s. The flow velocity of each material is in this case supersonic relative to the stagnation point (i.e., $V - U > C_{oj}$ and $U > C_{ot}$), and a standing shock is set up on either side of the stagnation point. Figure 8 is a pressure-velocity diagram of this case. For the incompressible theory, the Bernoulli curves intersect at a penetration velocity of 4.65 km/s. For the compressible theory, the presence of the shocks means that station 0_j is distinct from 1_j, and 0_t from 1_t. The changes in properties between each pair of points are given by the Rankine-Hugoniot conditions, which define the Hugoniot curve of each material, as shown in the figure. The actual locations of points 1_j and 1_t depend on the strengths of the shocks, which are determined by the penetration velocity U and are therefore unknown until the conditions at the stagnation point have been found (this explains why an iterative technique is required to solve the entire problem). Between stations 1 and 2, each material is compressed and decelerated according to the compressible Bernoulli's equation and the isentropic condition. The intersection of these Bernoulli isentropes in the figure gives the conditions at the stagnation point; in this case, the penetration velocity $U_{compressible}$ = 4.62 km/s, only slightly less than the incompressible value.

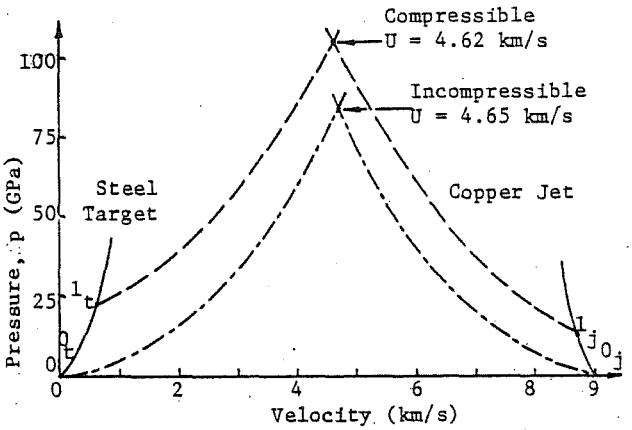

Figure 8. Pressure-velocity diagram for penetration of a copper jet into a steel target at 9 km/s.

When the target is much more compressible than the jet, as in the case of a copper jet penetrating Plexiglas, the situation is quite different, as shown in Figure 9. The incompressible theory predicts the penetration velocity $U_{incompressible}$ = 5.86 km/s for a jet velocity V = 8 km/s. Taking compressibility into account, note that the flow is subsonic in the jet ($V - U < C_{oj}$) but supersonic in the target ($U > C_{ot}$); therefore, a standing shock exists in the target but not in the jet. Thus, in the target, the pressure first jumps from 0_t to 1_t according to the Hugoniot of Plexiglas, then increases along the Bernoulli isentrope to its stagnation value at point 2. In the jet, there is no distinction between 0_j and 1_j, and the entire increase in pressure follows the Bernoulli isentrope. The penetration velocity is $U_{compressible}$ = 5.52 km/s, 5.6% less than the incompressible value. By equation (11), this corresponds to an 18% reduction in penetration per unit length of jet.

Stretching Jets

For a stretching jet (of non-uniform velocity distribution), the effect of compressibility may be considerably amplified. The

reason for this is that, if the penetration of the front portion of the jet is degraded even a little, the rear will have stretched less by the time it reaches the bottom of the crater. Since penetration is proportional to jet length, the rear of the jet also penetrates less. Furthermore, the degradation is cumulative over the length of the jet.

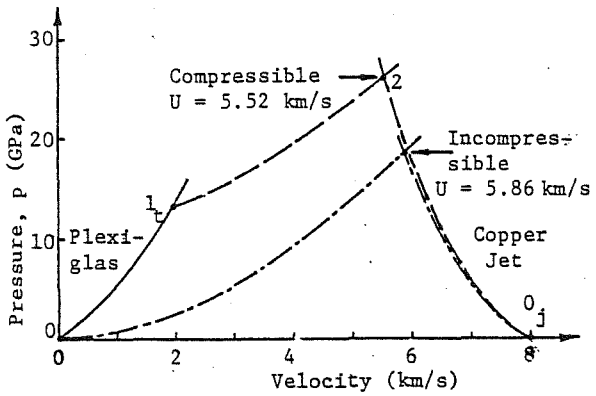

Figure 9. Pressure-velocity diagram for penetration of a copper jet into a Plexiglas target at 8 km/s.

Figure 10 presents calculated results for a stretching copper jet penetrating targets of steel and polyethylene. The ratio, calculated by equation (18), of penetration predicted by the compressible model to that by the classical incompressible model is plotted versus jet tip velocity; the tail velocity is fixed at 2.0 km/s. For the steel target, the results show that the effect of compressibility is slight, even for the stretching jet. For the polyethylene target, on the other hand, the compressible penetration may be as much as 45% less than the incompressible at practical shaped-charge jet velocities.

V. CONCLUSIONS

The one-dimensional compressible model of steady-state jet penetration of Haugstad and Dullum has been generalized to incorporate a complete equation of state to describe the jet and target materials. Calculated results confirm that compressibility has an appreciable effect (up to 20%) on the penetration per unit length of a uniform-velocity jet, when there is a significant difference in the compressibilities of the jet and target materials.

The model has been extended to the case of a stretching jet, by taking advantage of the virtual-origin approach to describe the jet-velocity distribution. Calculated results here indicate that the effect of compressibility is amplified in a stretching jet, yielding up to a 50% decrease in penetration, relative to the classical, incompressible, hydrodynamic model of penetration, for very compressible target materials.

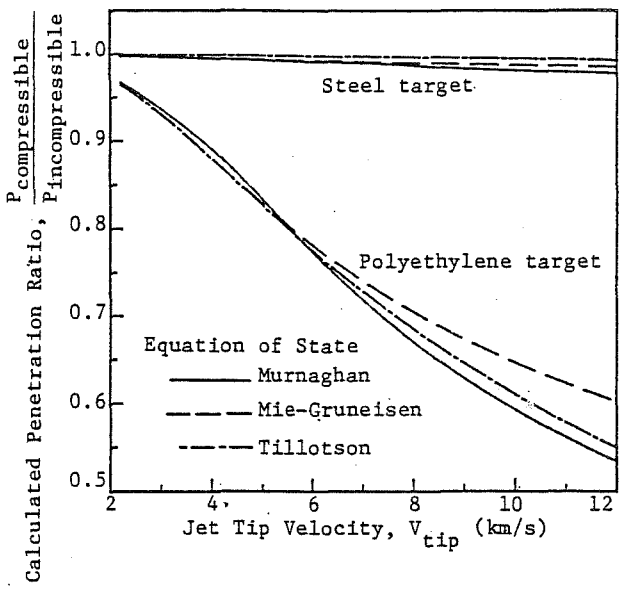

Figure 10. Effect of compressibility of penetration of a stretching copper jet of 2-km/s tail velocity against steel and polyethylene targets, as predicted using different equations of state.

VI. ACKNOWLEDGMENT

This research was supported by the U.S. Air Force Armament Laboratory under the Jet-Target Interaction Study, Contract No. F08635-82-C-0215.

VII. REFERENCES

1. Allison, F.E., and Vitali, R., "A New Method of Computing Penetration Variables for Shaped-Charge Jets," BRL Report No. 1184, 1963.

2. Harlow, F.H., and Pracht, W.E., "Formation and Penetration of High-Speed Collapse Jets," The Physics of Fluids, V. 9, No. 10, 1966.

3. White, J.J.; Wahll, M.J.; and Backofen, J.E., "Observation of Compressibility-Related Effects in Shaped-Charge Jet Penetration," J. App. Phys., V. 53, No. 6, 1982.

4. Birkhoff, G.; MacDougall, D.P.; Pugh, E.M.; and Taylor, G., "Explosives with Lined Cavities," J. Appl. Phys., V. 19, 1948.

5. Eichelberger, R.J., "Experimental Tests of the Theory of Penetration by Metallic Jets," J. Appl. Phys., V. 27, 1956.

6. Haugstad, B.S. and Dullum, O.S., "Finite Compressibility in Shaped Charge Jet and Long Rod Penetration--The Effect of Shocks," J. Appl. Phys., V. 52, No. 8, 1981.

7. Murnaghan, F.D., "The Compressibility of Media Under Extreme Pressures," Proc. Nat. Acad. Sci., V. 30, 1944.

8. Bridgman, P.W., "Compressions and Polymorphic Transitions of Seventeen Elements to 10^5 kg/cm^2," Phys. Rev., V. 60, 1941.

9. Kohn, B.J., "Compilation of Hugoniot Equations of State," U.S. Air Force Weapons Lab., Tech. Rept. No. AFWL-TR-69-38, 1969.

10. Tillotson, J.H., "Metallic Equations of State for Hypervelocity Impact," General Atomic Report GA-3216, 1962.

11. Rice, M.H. and Walsh, J.M., "Equation of State of Water to 250 Kilobars," J. Appl. Phys., V. 26, 1957.

12. Haugstad, B.S., "Compressibility Effects in Shaped Charge Jet Penetration," J. Appl. Phys., V. 52, No. 3, 1981.